Active Control of the Wave-Induced Motions of a Float: Real-Time Simulations with a Digital Twin and Experimental Validation

Stephanie C. Steele[1], *Shawn Albertson*[1], *Jacob Fontaine*[1], *Jason M. Dahl*[1],
Stephan T. Grilli[1], *Reza M. Hashemi*[1], *Yuksel R. Alkarem*[2,3], *Richard W. Kimball*[4], *Babak Hejrati*[4]
(1) Department of Ocean Engineering, University of Rhode Island Narragansett, RI, USA
(2) Department of Civil and Environmental Engineering, University of Maine Orono, ME, USA
(3) Advanced Structures & Composites Center, Orono, ME, USA
(4) Department of Mechanical Engineering, University of Maine, Orono, ME USA

ABSTRACT

Floating offshore structures, which are subject to wave-induced motions, are used in a wide range of ocean engineering applications, from vessels of various sizes, to oil and gas platforms (TLPs, simply tethered, . . .), and more recently, floating offshore wind turbine (FOWT) design concepts. To optimize a variety of design and operational factors, it is important to minimize these wave-induced motions, which in some cases may require using semi- or fully-active methods that may use phase-resolved information about incoming waves. In the latter case, a mass or water ballast can be actuated or moved by a pump to counteract effects of the wave-induced forces and moments on the float, on the basis of some control law. Here we present the development and experimental validation of a control system based on real-time simulations of the wave-induced motions of a floating object, with its active control method, using a complete physics-based model, referred to as a digital twin (DT). For demonstration and validation, the system is applied to a barge-like float, for which a 1:19.22 scale model is tested in a laboratory wave tank (30 m long, 3.6 m wide and 1.8 m deep) in our facilities, while being placed transverse to the tank axis, in regular or irregular waves. The float is equipped with a nonlinear model predictive controller based on a mass moving horizontally on a slider in the barge's beam direction to control its rolling motion, actuated by a linear motor. The controller is actuated based on the DT modeling of float heave and roll including the effect of the moving mass, informed by the assimilation of past float motions and, optionally, using phase-resolved wave data at the float (either measured or predicted based on a separate model) incorporating disturbance previewing in the controller. In the experiments, the complete system is implemented and run in realtime on a desktop computer. Results will be presented and discussed, showing a significant reduction in float motions when the active control method is used. Considerations for using a similar concept to control FOWT motions will be presented as well as the potential for using open source software (OpenFAST) as a real time DT.

KEYWORDS: Hydrodynamics modeling; dynamic positioning; control; model predictive control; model test.

INTRODUCTION

The development of Floating Offshore Wind Turbine (FOWT) infrastructure along both the U.S. East and West coasts has recently accelerated, with the award of many lease areas for large scale farm implementations. While the wide continental shelf along much of the U.S. East Coast has supported the development of fixed structure wind turbines, deeper waters in the Gulf of Maine and along the U.S. Pacific Coast are more suitable to floating systems, which can be more economically deployed and take advantage of the vast offshore wind energy resource in these regions. The operations of wind turbines are highly sensitive to their orientation with respect to wind direction, hence FOWTs, which are subject to wave-induced motions, offer significant operational challenges since dynamic motions of the float can introduce changes to orientation of turbine blades with respect to the wind direction, imbalance of loads on the generator, and added fatigue damage to the structures, amongst others.

The real time control and minimization of the motions of a large, anchored, FOWT subject to dynamic environmental forces in irregular sea state and wind conditions is a complex multi-faceted problem that has only been partially researched (Martin, Kimball, Viselli, and Goupee (2013); Viselli, Dagher, and Goupee (2015); Viselli, Dagher, Goupee, and Allen (2015); Viselli, Forristall, Pearce, and Dagher (2015)). While many studies of active control of wind loading effects have been done for onshore and offshore wind turbines focusing on turbine control (Raach, Schlipf, Sandner, Matha, and Cheng (2014)), less work has been devoted to controlling wave-induced motions. Strategies for controlling float motions may involve passive techniques, such as tuned mass dampers (TMDs), which may use optimized spring-mass systems to mitigate float vibrations (Verma, Nartu, and Subbulakshmi (2022)), however passive techniques may not be sufficient for suppressing motions in a broad-band irregular wave environment.

Alternately, active control techniques may be used, which besides assimilating past float motions, for more accuracy, require predicting in the short term, both the wave loading on the FOWT and the float response to it (e.g., Ma, Sclavounos, Cross-Whiter, and Arora (2018)). Based on such predictions, the dynamic motions of the FOWT may then be actively controlled, for instance, by moving water or solid ballast within the float.

For instance, Wakui, Nagamura, and Yokoyama (2021) present a model predictive controller for a FOWT that uses wind speed and wave height as inputs. To predict the latter, they use a linear time-invariant identified model.

In this study, given a wave remote sensing method (here assumed Lidar-like; e.g., Nouguier, Grilli, and Guérin (2014)) that can acquire dense spatio-temporal data sets of wave surface elevations at a short distance from the float (e.g., 100-200 m in the incident wave direction), we apply a local wave reconstruction and prediction (WRP) algorithm, based on deterministic phase-resolved wave models, that can accurately predict future wave elevations at the float in an irregular sea state. Previous work has demonstrated the efficiency of using Lagrangian, rather than Eulerian, wave models to do so, and the importance of including nonlinear amplitude dispersion effects in the models to accurately predict wave phases at the float (Desmars, Bonnefoy, Grilli, Ducrozet, Perignon, Guérin, and Ferrant (2020)). While active control of a floating system can be implemented over different time scales (e.g., long time scales on the order of changes to the local wave spectrum vs. short time scales on the order of individual wave characteristics), the present study focuses on control strategies at relatively short time scales (e.g., near-term of order 10-15 s at full scale), utilizing measurement and prediction of local, near-field wave conditions for implementation in a control system. Based on earlier work (Desmars, Bonnefoy, Grilli, Ducrozet, Perignon, Guérin, and Ferrant (2020)), the WRP algorithm used in the control system uses the nonlinear Lagrangian "Choppy" wave model, with improved nonlinear dispersion properties, and its implementation and validation for real time predictions at the float are detailed in the complementary paper by Albertson, Gharankhanlou, Steele, Grilli, Dahl, Grilli, Hashemi, Alkarem, and Huguenard (2023), also presented in this program.

In addition to the WRP algorithm, the control system is informed by simulations with a digital twin (DT) model of the wave-induced float motions. Based on earlier work by Grilli, Dahl, Grilli, and Steele (2018) and Grilli, Grilli, Bastien, Sepe Jr., and Spaulding (2011), the DT model solves for the real time heave, roll, and pitch motions of the float, given wave excitation and other loads affecting the float dynamics (e.g., for a FOWT this would be wind loads). Following the approach proposed by Babarit and Clément (2006), and applied by Grilli, Dahl, Grilli, and Steele (2018) and Grilli, Grilli, Bastien, Sepe Jr., and Spaulding (2011), we use the Prony approximation method to transform the computation of the "memory term" convolution integrals, that are part of the equations governing the wave-induced float motions in the time domain, into additional ordinary differential equations (ODEs) that become part of the solution of a larger system of ODEs. While similarly accurate, this approach was shown to be more efficient than solving integro-differential equations, which is important for the real time implementation of the DT model.

In this study, for the first time, we demonstrate the addition of wave motions in the control of a float in real-time towards the application of including wave motion predictions in actively controlled FOWT. The focus on wave motions enables control not only on blade motions, but also on overall float motions, which allows insight and control based on instrinsic aspects of FOWT operation such as fatigue life and effects of float motions on energy production.

FLOAT SYSTEM

The real time active control system, with DT-WRP models, is implemented and validated based on laboratory experiments performed in the University of Rhode Island wave tank (30 m long, 3.6 m wide and 1.6 m deep), with a float system representing the 1:19.22 scale model of a barge-like tug boat. Fig. 1 shows the side and front view of the lab scale float system, with length $L = 1.37$ m, maximum draft $D = 0.1262$ m, operating draft $d = 0.0385$ m, and beam width $B = 0.38$ m. The float is

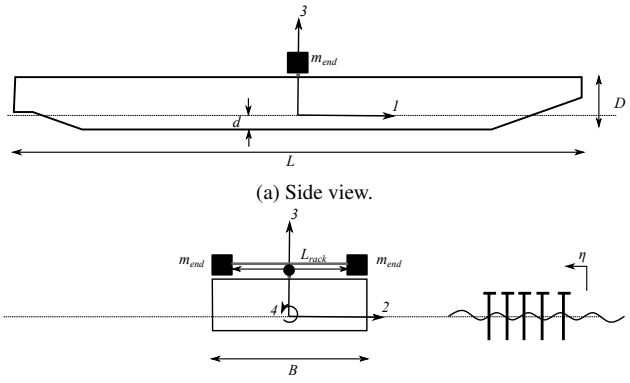

(a) Side view.

(b) Front view.

Fig. 1: Views of the float system, and its main dimensions, as deployed and tested in heave and roll in laboratory experiments. The 5 vertical T's marked in (b) denote locations of wave gauges where incident wave elevations $\eta(x,t)$ are measured, which are used in the WRP algorithm. The black squares are masses located on a slider actuated by a motor, with rack and pinion, for the real time control of the float rolling motions.

Fig. 2: A view of the entire experimental configuration. Wave gauges placed in the bottom right measure wave elevations and feed them into the NI DAQ. The float can be seen mounted to the carriage in the top left.

constrained to move in only heave and roll, referred to as the directions 3 and 4, respectively, as is standard in floating body dynamics. Unidirectional periodic or irregular waves are propagating towards the float, i.e, at an incidence angle of 90° from the longitudinal axis of the float (beam seas). The heave position and roll angle are measured by two onboard string potentiometers attached to the tank tow carriage. Wave gauges are placed upstream of the float to predict and supply the WRP model with incoming wave information. Fig. 2 shows the wave tank with the float placed in it, the tow carriage above it and the wave gauges upstream of it. Lastly, a horizontal rack and pinion slider system is mounted on top of the float hull of rack length L_{rack} and masses at either end m_{end} to exert roll restoring moments as dictated by the control system (Fig. 1b). Fig. 3 shows a close-up of the moving ballast mechanism mounted to the deck of the model float. The moving ballast control is meant to provide a proof of concept control system, simulating the effect of a moving fluid ballast system.

DIGITAL TWIN MODEL

The DT is comprised of a nonlinear model for predicting the motions of the float system based on incident wave characteristics at the float, as well as an extended Kalman filter to estimate the float system states $\hat{x}$ that are

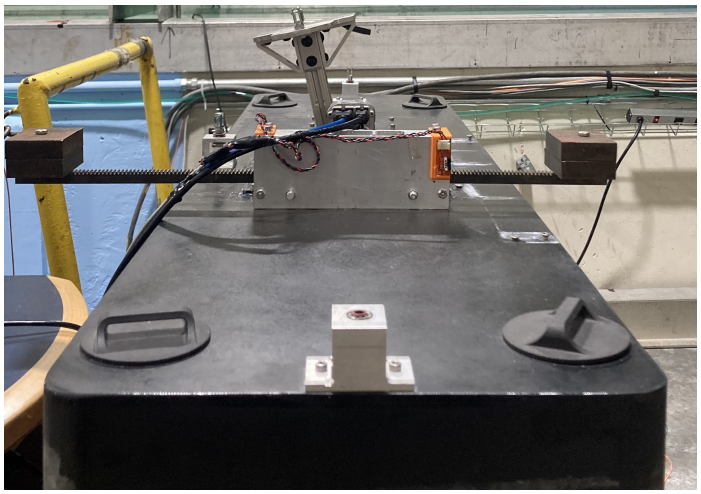

Fig. 3: Close-up of close-up of the moving ballast mechanism mounted to the deck of the model float. The aluminum frame houses the motor and rack pinion interface, while the square masses can be seen protruding past the edge of the barge on either side. The attachment to the wave tank carriage is made via the aluminum plate at the top of the image.

not directly measured. These models are shown within the orange box in the control system block diagram of Fig. 4.

Equations of Motion

To develop the nonlinear floating body dynamics model and identify the states for the float system, we express the float equations of motion for heave and roll, respectively, as $(i, j = 3,4)$,

$$\left(M_{ij}+A_{ij}(\infty)\right)\ddot{\zeta}_j+\int_0^t K_{ij}(t-\tau)\,\dot{\zeta}_j\,\mathrm{d}\tau+F_i^H(\zeta_i,\eta)+F_i^D(\dot{\zeta}_j)=F_i^E+F_i^C \tag{1}$$

where $\zeta_i(t)$ is the instantaneous ship displacement in meters for heave and radians for roll, M_{ij} and $A_{ij}(\infty)$ are the ship mass or inertia and added mass or inertia values at infinite frequency. The convolution integral represents the motion memory terms, which are a function of the impulse response functions (IRFs) $K_{ij}(t)$. $F_i^H(\zeta_i,\eta)$ is the total hydrostatic restoring force or moment, which is a nonlinear function of the float displacements and instantaneous surface elevation $\eta(t)$. $F_i^D(\dot{\zeta}_i)$ is a nonlinear viscous damping force or moment as a function of the float velocities. F_i^E is the instantaneous excitation force from incident waves. F_i^C is the instantaneous control force exerted on the float system by the control system. The equations of motion in Eq. 1 are based on standard linearized seakeeping equations of motion such as presented in Lewis (1989), with modifications including the convolution terms, which capture wave memory effects on float motions in irregular seas, and the addition of a nonlinear component to the hydrostatic restoring force in heave, a nonlinear viscous damping terms in both heave and roll, and the controller forcing.

Note, as there is no significant dynamic coupling between the heave and roll motions for the considered float model, the hydrodynamic coefficients A_{ij} and B_{ij}, and the resulting IRFs (see below) are equal to zero for $(i \neq j)$. Considering symmetries in geometry and mass distribution, the mass and inertia matrix $M_{ij} = 0$ for $(i \neq j)$.

Approximating the Memory Term

Based on Cummins' (1962) work on linear seakeeping theory, the IRFs are defined for each degree of freedom based on the linear added mass $A_{ii}(\omega)$ and damping $B_{ii}(\omega)$ coefficients, dependent on the incident wave angular frequency ω, according to two possible forms as,

$$K_{ii}(t) = -\frac{2}{\pi}\int_0^\infty \left(A_{ii}(\omega)-A_{ii}(\infty)\right)\omega\sin(\omega t)\,\mathrm{d}\omega \tag{2}$$

$$= \frac{2}{\pi}\int_0^\infty \left(B_{ii}(\omega)-B_{ii}(\infty)\right)\cos(\omega t)\,\mathrm{d}\omega. \tag{3}$$

The IRFs are computed by numerical integration, using the frequency-dependent hydrodynamic added mass and radiative damping coefficients pre-calculated in AQWA. Analytical computations are made for the high-frequency tail of the integrals in Eq. (2) and (3), beyond some high-frequency cut-off.

As indicated, the Prony approximation method is used to transform the computation of the memory term convolution integral into the computation of the solution of a system of coupled ordinary differential equations (ODEs). Thus, we pose,

$$K_{ii}(t-\tau)=\sum_{p=1}^{P}\beta_{p,ii}\,\mathrm{e}^{S_{p,ii}(t-\tau)}, \tag{4}$$

where P is the order of the Prony approximation, and $\beta_{p,ii}$ and $S_{p,ii}$ are complex Prony coefficients, which are computed as least square fit to the results of Eq. (2) or Eq. (3). Then, using Eq. (4), the memory terms in Eqs. (1) are approximated as,

$$\int_0^t K_{ii}(t-\tau)\,\dot{\zeta}_i(\tau)\,\mathrm{d}\tau=\Re\sum_{p=1}^{P}\beta_{p,ii}\int_0^t \mathrm{e}^{S_{p,ii}(t-\tau)}\,\dot{\zeta}_i(\tau)\,\mathrm{d}\tau=\Re\sum_{p=1}^{P}\beta_{p,ii}I_{p,ii}, \tag{5}$$

where we define the unknown complex functions $I_{p,ij}(t)$ as

$$I_{p,ii}\equiv \mathrm{e}^{S_{p,ii}t}\int_0^t \mathrm{e}^{-S_{p,ii}\tau}\,\dot{\zeta}_i(\tau)\,\mathrm{d}\tau. \tag{6}$$

Then taking the time derivative of the unknown complex function $I_{p,ij}(t)$,

$$\dot{I}_{p,ii}=S_{p,ii}I_{p,ii}+\mathrm{e}^{S_{p,ii}t}\frac{\mathrm{d}}{\mathrm{d}t}\{\int_0^t \mathrm{e}^{-S_{p,ii}\tau}\,\dot{\zeta}_i(\tau)\,\mathrm{d}\tau\} \tag{7}$$

and applying the Leibnitz theorem, we write P additional complex ODEs:

$$\dot{I}_{p,ii}=S_{p,ii}I_{p,ii}+\dot{\zeta}_i, \tag{8}$$

for each degree of freedom $(i = j = 3,4)$, i.e., $2P$ additional equations with as many new unknown complex functions $I_{p,ii}(t)$, to be found from the simultaneous solution of the ODEs coupled with Eqs. (1).

Hydrostatic Restoring Term

The hydrostatic force F_3^H and moment F_4^H,

$$F_3^H = C_{33}(\xi)\,\zeta_3+C_{34}\sin\zeta_4,$$
$$F_4^H = C_{43}\zeta_3+C_{44}\sin\zeta_4, \tag{9}$$

restore the heave and roll motion of the float, respectively, where $C_{33}(\xi)\,\zeta_3$ is the restoring force in heave caused by displacement in heave and is nonlinear due to the significant change of float length at the waterline depending on the relative heave motion $\xi=\zeta_3-\eta$ to the instantaneous surface elevation η. $C_{34}\sin\zeta_4$ is the restoring force in heave caused by displacement in roll while $C_{43}\zeta_4$ is the restoring moment in roll caused by displacement in heave. $C_{44}\sin\zeta_4$ is the restoring moment in roll caused by displacement in roll. C_{34}, C_{43}, and C_{44} are coefficients previously obtained through hydrodynamic simulations of the hull form in AQWA. The nonlinear coefficient $C_{33}(\xi)$ is calculated as

$$C_{33}(\xi)=\rho\,g\,B\,L_w(\xi), \tag{10}$$

where ρ is the water density, g is the gravitational constant, and the length of the float at the waterline $L_w(\xi)$ is a nonlinear function:

$$L_w(\xi) = \begin{cases} 1.1722 + 5.893\,\xi & -d < \xi \le 0.0395 - d \\ 1.1866 + 2.979\,\xi & 0.0395 - d < \xi \le 0.0789 - d \\ 1.3195 & 0.0789 - d < \xi \le D - d, \end{cases} \tag{11}$$

Viscous Damping Term

The nonlinear viscous damping force and moment,

$$F_3^D = b_{D3}\dot{\zeta}_3|\dot{\zeta}_3|$$
$$F_4^D = b_{D4}\frac{B}{2}\dot{\zeta}_4|\frac{B}{2}\dot{\zeta}_4| \tag{12}$$

for heave and roll, respectively, are included in Eqs. (1) to simulate the effects of vortex shedding and skin friction resulting from large amplitude float motions in heave and roll. These are standard empirical expressions, proportional to the square of the motion velocity and coefficients, $b_{Di} = (1/2)\rho\, C_{Di} S_{Hi}$, with S_{Hi} a relevant wetted surface area or static moment, and C_{Di} a drag coefficient. We define $S_{H3} = 2d(B+L)$ in heave and $S_{H4} = LdB$ in roll. Coefficients C_{Di} are calibrated by comparing model results to scale model testing.

Excitation Term

The excitation force or moment F_i^E for irregular waves can be expressed as a linear superposition over the number of frequency components N_ω that have significant energy in the incident wave, with incident wave amplitude a_n and phase φ_n components:

$$F_i^E(t) = \sum_{n=1}^{N_\omega} a_n R_{i,n} \cos\left(\omega_n t + \alpha_{i,n} + \varphi_n\right), \tag{13}$$

where $R_{i,n}(\omega_n)$ and $\alpha_{i,n}(\omega_n)$ are the interpolated amplitude and phase, respectively, of the excitation force or moment in heave and roll for each individual wave component of unit amplitude, previously computed in AQWA, for discrete regular waveforms.

Controller Forcing Term

The control moment exerted in the roll direction F_4^C is a quasi-static moment based on the position $l(t)$ of the control rack as a function of time,

$$F_4^C = (2l - L_{rack})\, m_{end}\, g, \tag{14}$$

where $l = 0$ when the rack is positioned with its leftmost end mass nearly above the origin (Fig. 1b), and $l = L_{rack}$ when the rack is positioned with its rightmost end mass positioned nearly above the origin (the case of $l = L_{rack}/2$ is when the control rack is centered above the origin). The horizontally sliding control rack and pinion is modeled as exerting no quasi-static heave forces on the float. Additionally, dynamic effects from the moving masses are neglected.

Complete System of Seakeeping-control ODEs

To compute the float displacements in heave and roll as a function of time $\zeta_i(t)$, the system of 2 second-order ODEs (Eq. (1)), which can be written as 4 first-order ODEs and with the memory terms approximated by Eq. (5), is solved simultaneously with $2P$ real first-order ODEs (Eq. (8)) for each P complex Prony function $I_{p,ii}$. For $P = 4$ and two degrees of freedom in heave and roll, this yields a system of 20 first-order nonlinear ODEs to be solved at each time step of the model solution. The ODE system in total, for float displacements in heave and roll as a function of time $\zeta_i(t)$ $(i = 3,4)$, using velocities $V_i(t)$ as auxiliary variables, and with $p = 1, \ldots P$, reads:

$$\begin{aligned} \dot{\zeta}_i &= V_i \\ \dot{V}_3 &= -\frac{1}{M_3}\left\{\Re\sum_{p=1}^{P}\beta_{p,33} I_{p,33} + F_3^H(\zeta_i,\eta) + b_{D3}V_3|V_3| - F_3^E(t)\right\} \\ \dot{V}_4 &= -\frac{1}{M_4}\left\{\Re\sum_{p=1}^{P}\beta_{p,44} I_{p,44} + F_4^H(\zeta_i) + b_{D4}\frac{B^2}{4}V_4|V_4| \right. \\ &\qquad \left. - F_4^E(t) - F_4^C(t)\right\} \\ \dot{I}_{p,ii} &= S_{p,ii} I_{p,ii} + V_i \end{aligned} \tag{15}$$

where the total mass or inertia terms are defined as,

$$M_3 = (M_{33} + A_{33}(\infty)); \qquad M_4 = (M_{44} + A_{44}(\infty)). \tag{16}$$

Eq. (15) can now be used as a full nonlinear DT model predicting the wave-induced motions of the float for given incident waves (i.e., here, such as predicted at the float using he WRP algorithm). Lastly, for the model to be compatible with an extended Kalman filter, in order to estimate the float system states that are not directly measured, we recognize Eq. 15 to be in the form of a nonlinear system of equations $\dot{\mathbf{x}} = f(\mathbf{x})$ with the state vector $\mathbf{x}$ of the float system identified as, with a total of 20 states,

$$\mathbf{x} = [\zeta_i; V_i; \Re(I_{p,ii}); \Im(I_{p,ii})]. \tag{17}$$

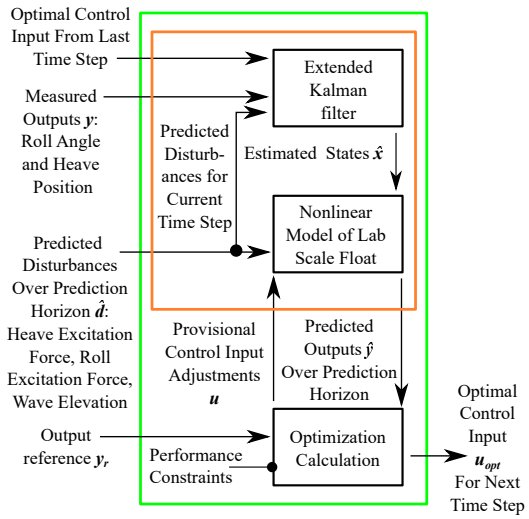

Fig. 4: Nonlinear model predictive controller (MPC) block diagram. Components within the orange box include the digital twin (DT) model of the lab scale float, with wave prediction using the WRP model. Components in the green box are the nonlinear model predictive control system.

CONTROL SYSTEM

The control system is run in a closed-loop manner, incorporating real-time sensor measurements of heave and roll displacements and wave characteristics predictions with previewing. The control system is a nonlinear model predictive controller (MPC), representing an optimization problem with information from a DT model of the float system, which chooses a control action (subject to constraints) that minimizes a specified cost function. Here, the MPC is nonlinear, because the DT model it

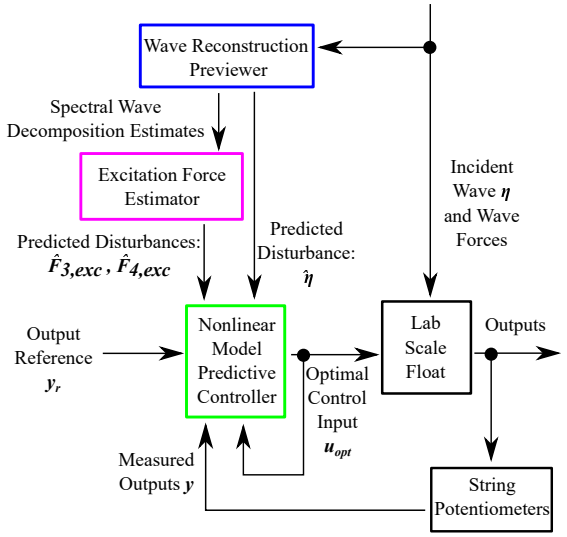

Fig. 5: Block diagram of overall system including nonlinear model predictive controller (MPC), wave reconstruction previewer (WRP), excitation force database estimator, and physical / simulated lab scale float model.

obtains information from is a nonlinear model (Eqs. (15)). We also employ disturbance previewing in the control system, in which measured disturbances are predicted for future times over a prediction horizon h_p. The controller is implemented in MATLAB, with objects and functions from the Model Predictive Control Toolbox and Control System Toolbox.

Figure 5 shows the block diagram of the overall control system. Incident waves that have not arrived yet at the float are measured upstream of the float (here using wave gauges), and the wave reconstruction previewer (WRP) model predicts the wave elevation and spectral components that will reach the float by the time the wave content has propagated to the float (see Albertson, Gharankhanlou, Steele, Grilli, Dahl, Grilli, Hashemi, Alkarem, and Huguenard (2023)). Since these predictions are made before the wave content has reached the float, we have near-term predictions of the future wave elevation and wave components at the float, i.e. previewing. The previewed spectral components, which are direct components of the WRP wave model representations (see, Albertson, Gharankhanlou, Steele, Grilli, Dahl, Grilli, Hashemi, Alkarem, and Huguenard (2023)) are used to estimate future excitation forces as well using Eq. (13). The predicted preview of the wave elevation and excitation forces in heave and roll are used as input to the DT model of the float, within the nonlinear MPC. Meanwhile, the incident wave eventually reaches the float system, which reacts with motions in heave and roll (the only unconstrained degrees of freedom allowed here). The heave and roll angle displacements are measured by the onboard string potentiometers, which provide feedback input to the MPC. The output reference, in this case a constant value of zero roll angle, as well as the previous control action, are also input to the controller, which incorporates all its inputs to send a control action command to the lab scale float, which actuates the mass/rack/slider system accordingly, thus completing the feedback with previewing loop.

Optimization Control Law

The nonlinear MPC in the control system is comprised of the nonlinear DT model of the float system and an extended Kalman filter to estimate the unmeasured float system states (the digital twin) as well as an optimization calculation that minimizes motions in roll, as shown inside the green box in Fig. 4.

The optimization problem is expressed as a quadratic problem, whose solution is the control decision that minimize the cost function subject to constraints, in this case the control rack position $l(t)$. The cost function $J(z_k)$ is comprised of three cost function components,

$$J(z_k) = J_{\zeta_4}(z_k) + J_{\Delta l}(z_k) + J_{\varepsilon}(z_k), \tag{18}$$

where $J_{\zeta_4}(z_k)$ is the roll angle tracking cost function component, $J_{\Delta l}(z_k)$ is the control rack position rate tracking cost function component, and $J_{\varepsilon}(z_k)$ is the constraint softening cost function component. The optimization problem decision is, $z_k^T = [l(k|k)^T l(k+1|k)^T ... l(k+h_p-1|k)^T \varepsilon_k]$, where control rack positions $l(k+i|k)$ over the prediction horizon h_p with $i = 0...h_p-1$ as well as the slack variable ε_k at each control interval k are freely optimized as optimization variables (we set the control horizon equal to the prediction horizon).

The roll angle reference tracking cost function component reads,

$$J_{\zeta_4}(z_k) = \sum_{i=1}^{h_p} \left(\zeta_{4,ref} - \zeta_4(k+i|k)\right)^2, \tag{19}$$

where we desire a constant reference roll angle, $\zeta_{4,ref} = 0$, and $\zeta_4(k+i|k)$ is the predicted roll angle at the ith prediction horizon step.

The control rack position rate tracking cost function component reads,

$$J_{\Delta l}(z_k) = \sum_{i=0}^{h_p-1} \{w_i^{\Delta l} \left(l(k+i|k) - l(k+i-1|k)\right)\}^2, \tag{20}$$

where the control rack position rate weight is set small at $w_i^{\Delta l} = 0.02$, to slightly smooth out controller action rates of change, which in general needs to be considered on controller hardware.

The constraint softening cost function component reads,

$$J_{\varepsilon}(z_k) = \rho_{\varepsilon} \varepsilon_k^2, \tag{21}$$

with constraint violation penalty weight $\rho_{\varepsilon} = 10^5$. As a note, a larger ρ_{ε} value relaxes the constraints on roll angle tracking and control rack position rate tracking.

Nonlinear Model Predictive Controller Settings

A nonlinear model predictive controller object is implemented in MATLAB with 20 states according to Eq. 17, 2 measured outputs of heave and roll, 3 measured disturbances of excitation force in heave, excitation force in roll, and wave elevation, and an internal model of the float according to Eq. 15. The control horizon is set equal to the prediction horizon, which we will vary in the results. Lastly, hard constraints are set on the control rack position according to its physical limits of a minimum of 0 and a maximum of L_{rack}.

Measured Disturbances

The measured disturbances are specified as inputs that will perturb the float system. For our digital twin, we have specified the heave excitation force, the roll excitation force, and the wave elevation as the measured disturbances into the system. The measured disturbances are also previewed for future values, as inputs to the optimization calculation over the prediction horizon. The previewed heave and roll excitation forces act as a force input to the digital twin, whereas the previewed wave elevations act to update the future nonlinear C_{33} restoring coefficients within the digital twin model.

To preview both the excitation forces and the wave elevation, we need to predict and propagate wave characteristics upstream of the float to future instances in time. This is achieved through a Wave Reconstruction and Prediction (WRP) algorithm, where upstream spatio-temporal measurements of waves are used to reconstruct wave characteristics some

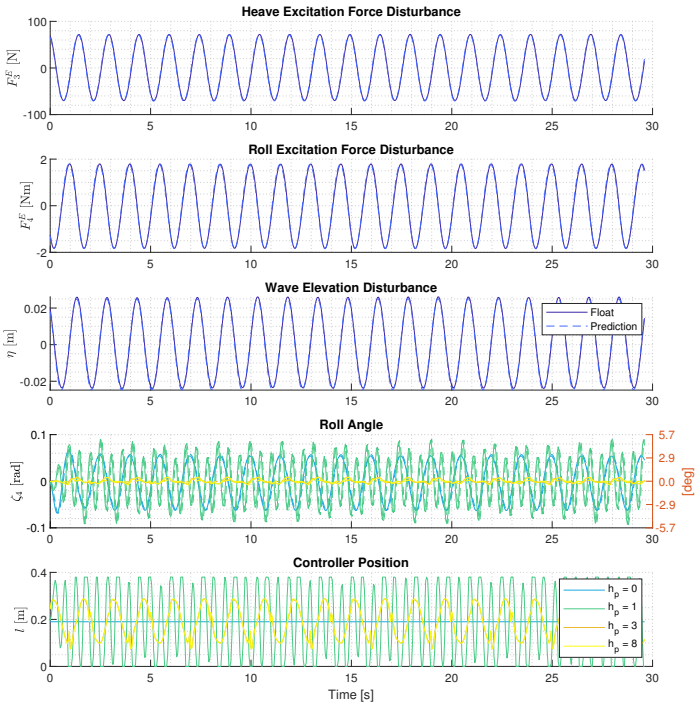

Fig. 6: Float and predicted heave excitation force, roll excitation force, wave elevation, roll angle with varying prediction horizons h_p, and corresponding control rack positioning l for periodic incident waves of wave height $H = 0.05$ m and period $T = 1.5$ s.

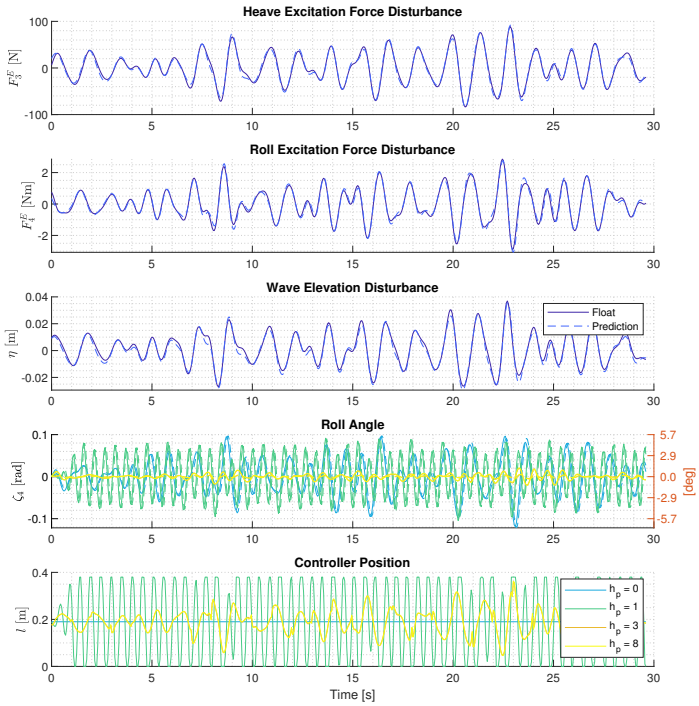

Fig. 7: Float and predicted heave excitation force, roll excitation force, wave elevation, roll angle with varying prediction horizons h_p, and corresponding control rack positioning l for irregular incident waves of significant wave height $H_s = 0.05$ m and peak period $T_{peak} = 1.5$ s.

distance away from the float, then propagated to the location of the float for input to the DT model. The method for implementing this algorithm follows that of Desmars, Bonnefoy, Grilli, Ducrozet, Perignon, Guérin, and Ferrant (2020) and is described in detail in the complementary paper by Albertson, Gharankhanlou, Steele, Grilli, Dahl, Grilli, Hashemi, Alkarem, and Huguenard (2023).

SIMULATION RESULTS

The closed-loop simulation of the float system, DT, measured disturbance previewing, nonlinear model predictive controller, and sensor feedback is implemented in MATLAB, according to the block diagram in Fig 5. First, float parameters such as overall dimensions, mass and inertia, constant restoring coefficients, and Prony coefficients are loaded into the DT.

Incident wave and prediction data is also loaded. To evaluate the controlled using simulated data, we use a Numerical Wave Tank (NWT) model from Nimmala, Yim, and Grilli (2013) to generate four sets of incident wave elevations, all with wave height or significant wave height input of 0.05 m, with two sets of irregular JONSWAP spectrum wave cases with peak periods $T_{peak} = 1.0, 1.5$ s and two periodic cases with periods $T = 1.0, 1.5$ s. The NWT is used to model nonlinear wave propagation, in this case in a flat-bottomed wave tank. Water depth was 1.4 m. Using the linear wave reconstruction modeling technique from Albertson, Gharankhanlou, Steele, Grilli, Dahl, Grilli, Hashemi, Alkarem, and Huguenard (2023), 3 virtual upstream measurements of wave elevations at locations 4.29 m, 3.85 m, 3.45m upstream of the float location are used to predict the wave elevation and its spectral components at the float location at later instances in time. The wave reconstruction previewer updates its predictions every 1 second.

From the simulated NWT data, we then have both a prediction of wave elevation (which includes a series breakdown of wave elevation and frequency components) and a true measured wave elevation (directly from the NWT) as input to the control model.

The extended Kalman filter (part of the digital twin) is initialized in order to estimate states from the nonlinear model (Eq. 15). The float motion is also simulated using the same nonlinear model Eq. 15.

The time-domain simulation is performed in which the predictions of the wave characteristics are updated, the measured disturbances are all previewed into the digital twin, the optimization problem solves for the optimal control adjustment, the optimal control adjustment is implemented on the float system, the extended Kalman filter predicts the estimated states of the float, the output sensor measurements of heave and roll displacements are taken, the output measurements are fed into the extended Kalman filter to correct its state estimates, and the process is repeated each time step. The controller sampling time (the time interval which elapses before the next controller loop process happens) is 0.05 seconds over a simulation duration of 30 seconds.

For each NWT data set, the closed-loop simulation is repeated for varying prediction horizons (time widths of future wave predictions). For each set of waves, we simulate a case with no control action whatsoever as a base case, one case with control but no previewing of measured disturbances, one case with a prediction horizon of 0.1 of one T_{peak} or T cycle (3 steps for $T, T_{peak} = 1.5$ s, 2 steps for $T, T_{peak} = 1.0$ s), and one case with a prediction horizon of 0.25 of one T_{peak} or T cycle (8 steps for $T, T_{peak} = 1.5$ s, 5 steps for $T, T_{peak} = 1.0$ s).

Figs. 6 - 9 show the simulation results for the periodic incident waves and irregular incident waves, respectively. The top three plots show, in order, the measured disturbance of the heave excitation force, the roll excitation force, and the wave elevation. Both the disturbance encountered at the float (solid line) and the predicted disturbance at the float (dashed line) are shown for each measured disturbance. The bottom two plots show the roll angle and controller position for the four control cases. The base case with no control is labeled as having prediction horizon $h_p = 0$

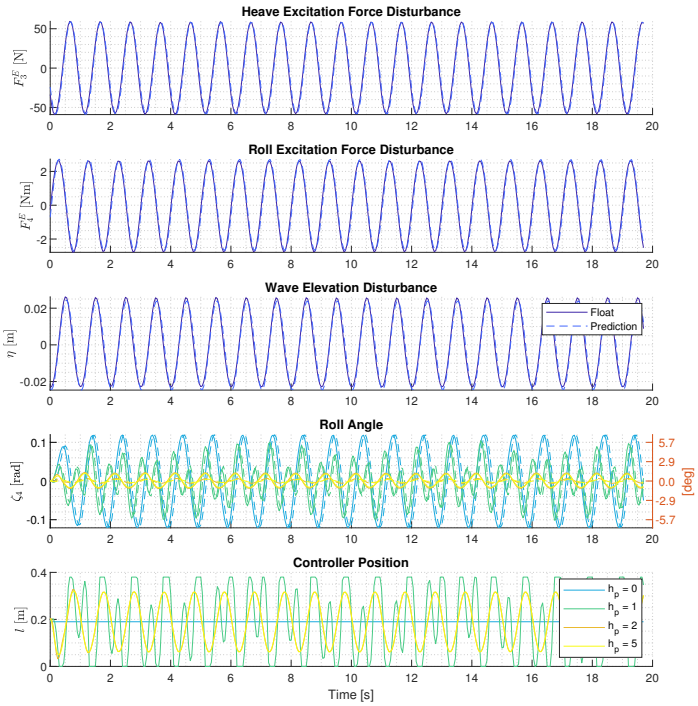

Fig. 8: Float and predicted heave excitation force, roll excitation force, wave elevation, roll angle with varying prediction horizons h_p, and corresponding control rack positioning l for periodic incident waves of wave height $H = 0.05$ m and period $T = 1$ s.

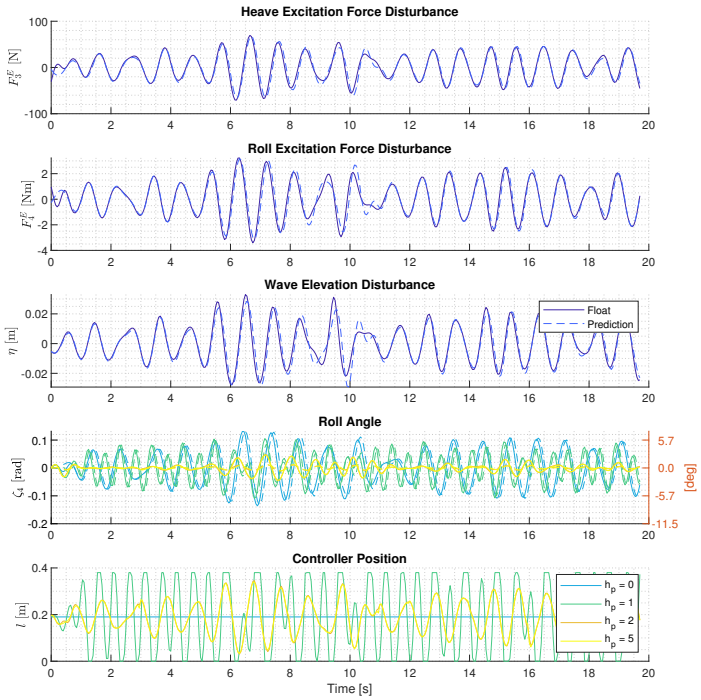

Fig. 9: Float and predicted heave excitation force, roll excitation force, wave elevation, roll angle with varying prediction horizons h_p, and corresponding control rack positioning l for irregular incident waves of significant wave height $H_s = 0.05$ m and peak period $T_{peak} = 1$ s.

(blue), the case with no previewing (current information only) is labeled with $h_p = 1$ (green), the case with previewing over the 0.1 cycle of T_{peak} is labeled with $h_p = 3$ for $T, T_{peak} = 1.5$ s or $h_p = 2$ for $T, T_{peak} = 1.0$ s (orange), and the case with previewing over 0.25 cycle of T_{peak} is labeled with $h_p = 8$ for $T, T_{peak} = 1.5$ s or $h_p = 5$ for $T, T_{peak} = 1.0$ s (yellow). For the roll angle, both the float roll angle (solid) and the extended Kalman filter state estimate (dashed) of the roll angle are shown, for each case of prediction horizon. The controller position l is shown on the bottom plot for each prediction horizon case.

The measured disturbance plots in Figs. 6 - 9 show that the prediction matches the actual disturbance at the float well, capturing the frequency content, phasing, and magnitude of the signals.

In the base cases with no control ($h_p = 0$, the maximum magnitude of roll angle in the periodic cases is about 3° and about 6° in the irregular cases. In both the periodic and irregular cases with no previewing ($h_p = 1$), the controller position oscillates at a faster rate than $1/T_{peak}$ (same as $1/T$) and the resulting roll angle is the same or larger as compared to the respective base cases. In the case of $h_p = 3$ for $T, T_{peak} = 1.5$ s and $h_p = 2$ for $T, T_{peak} = 1.0$ s, the controller position oscillates with period T in the periodic cases and oscillates much less rapidly in the irregular incident wave cases. For periodic and irregular incident waves, the roll angle is greatly reduced, to less than 1° in the cases for $T, T_{peak} = 1.5$ s, and less than about 2.5° for $T, T_{peak} = 1.0$ s, indicating significant improvement in desired roll positioning. Lastly, for the larger prediction horizons of $h_p = 8$ for $T, T_{peak} = 1.5$ s and $h_p = 5$ for $T, T_{peak} = 1.0$ s, the control action and the resulting roll angle look very similar to their corresponding results at $h_p = 3$ for $T, T_{peak} = 1.5$ s and $h_p = 2$ for $T, T_{peak} = 1.0$ s, where it is difficult to distinguish between these two cases as they lie nearly on top of one another. Thus, we see that for periodic and irregular incident waves, the digital twin and control system greatly reduce the float roll angle compared with float motions under no control, with previewing and a small prediction horizon.

The consequence of the float control working well even under a small prediction horizon that is only 1/10 of the peak period has positive practical implications for implementing this real time algorithm on a physical system. For example, forward looking LIDAR systems making measurements of the free surface will have a limited upstream range similar to the scaled distances evaluated in Albertson, Gharankhanlou, Steele, Grilli, Dahl, Grilli, Hashemi, Alkarem, and Huguenard (2023). However, with the control system working well over short prediction horizons, range limitations of the measurement system will have less effect on performance of the control algorithm.

EXPERIMENTAL VALIDATION

While the control algorithm has been demonstrated using simulated wave data and the digital twin of the model float system, real measurements and unmodeled differences between the digital twin and the physical system will introduce error into the control method. To demonstrate the control method applied to a physical system, we have planned a series of physical experiments using the model described earlier. The physical experiments will be conducted in the wave tank at URI.

For validation experiments, the model barge is oriented in the wave tank in order to experience beam seas as done previously in numerical experiments. The model is mounted to a heave staff allowing freedom to respond in heave. The heave staff connects to the model through roller bearings that also allow rotational motion of the model in roll. The heave staff rides on air bearings, allowing for extremely low frictional resistance of the experimental setup in heave. The roller bearings used for roll motion also have extremely low friction to limit the need for adjustment to the DT when comparing with model tests.

The moving ballast control system is shown attached to the existing model scale barge in Fig. 3. A single motor drives a rack and pinion holding the two moving masses. The smart servo motor uses position

commands as a direct input to drive the motor, hence the control developed previously for the DT can be used directly as input to control the physical position of the masses. The system is housed by an aluminum frame which serves to fix the mechanism to the barge.

The barge is designed to operate with a particular design draft. All previously calculations of hydrodynamic coefficients used for the DT model of the barge, assume that it operates with the design draft. While the static weight of the moving ballast system was designed to be as light as possible, the added weight to the model is more than the required ballast to reach the desired design draft, hence there is an increased draft for the model, which would result in a change to the hydrodynamic coefficients built into the DT. In order to maintain design draft for experiments, a constant force spring was added to the experimental fixture to offset the additional ballast weight. This has the effect of pulling the float out of the water to maintain design draft and keep the hydrodynamic coefficients the same. While this solution does not affect how the magnitude and distribution of mass contributes to the inertia, the inertia of the barge can easily be altered in the DT to match the inertia of the physical model.

The URI wave tank is capable of generating both periodic and irregular wave series with periods ranging from 0.5 s to 2 s and up to 15 cm amplitude. Wave gauges measure the wave elevation at particular points in space to be implemented for wave forecasting with the algorithm. Results from experimental validation will be presented during the presentation of this paper at the conference.

CONCLUSIONS

An algorithm is developed and demonstrated for controlling the roll motion of a floating platform, with applications directed for floating offshore wind turbine systems. The control method combines a digital twin model of the float system with a model predictive controller that incorporates future predictions of the wave elevation at the location of the float from distant measurements of the nearby wave elevation in both periodic and irregular sea states. The control algorithm is demonstrated using simulated wave data in a numerical wave tank demonstrating significant reduction in roll motions of the float when using future phase-resolved information about the incoming waves. Future experiments are planned to demonstrate the control method running in real time on a physical model undergoing similar wave forcing in a wave tank.

While the particular control method used to demonstrate this control algorithm involves a moving ballast system, this is implemented simply as a proof of concept demonstration of the real time algorithm. Future work will involve investigation of optimal methods of control, which may involve more complex moving ballast control, added mass control, and evaluation of energy cost in control methods. In addition, by implementing a DT model of the float system, more complex DT models can be investigated that incorporate other physical attributes of the floating offshore wind system, including power production, structural loading, and moorings. A more complex DT will enable other optimization points for the control system, such as minimization of fatigue damage or maximization of power output.

ACKNOWLEDGEMENTS

The authors gratefully acknowledge support for this work from grant # DE-SC0022103 of the United States Department of Energy (DOE).

REFERENCES

Albertson, ST, Gharankhanlou, M, Steele, SC, Grilli, ST, Dahl, JM, Grilli, AR, Hashemi, MR, Alkarem, YR, and Huguenard, K (2023). "Improved control of floating offshore wind turbine motion by using phase-resolved wave reconstruction and forecast." *In Proc. 33rd Intl. Offsh. and Polar Engng. Conf. ISOPE.*

Babarit, A, and Clément, AH (2006). "Optimal latching control of a wave energy device in regular and irregular waves" *Applied Ocean Res.*, 28, 77-91.

Cummins, WE (1962). "The impulse response function and ship motions", *Schiffstechnik*, 491-502.

Desmars, N, Bonnefoy, F, Grilli, ST, Ducrozet, G, Perignon, Y, Guérin, C-A, and Ferrant, P (2020). "Experimental and numerical assessment of deterministic nonlinear ocean wave prediction algorithms using non-uniformly sampled wave gauges.", *Ocean Engineering*, 212: 1037659.

Grilli, ST, Dahl, JM, Grilli, AR, and Steele, SC (2018). "Real-time sea-state estimation from inertial measurements of a ship's motions." *Proc. 16th Journée de l'hydrodynamique*, JH2018, Marseille.

Grilli, ST, Grilli, AR, Bastien, SP, Sepe Jr., RB, and Spaulding, ML (2011). "Small buoys for energy harvesting: Experimental and numerical modeling studies" *21st International Offshore and Polar Engineering Conference*, ISOPE, Maui, 598-605.

Lewis, EV (1989). *Principles of Naval Architecture: Volume 3*, SNAME, 51.

Ma, Y, Sclavounos, PD, Cross-Whiter, J and Arora, D (2018). "Wave forecast and its application to the optimal control of offshore floating wind turbine for load mitigation.", *Renewable Energy*, 128:163-176.

Martin, HR, Kimball, RW, Viselli, AM, and Goupee, AJ (2013). "Methodology for wind/wave basin testing of floating offshore wind turbines.", *J. Offshore Mech. and Arctic Engng*, 136(2):021902.

Nimmala, SB, Yim, SC, and Grilli, ST (2013)."An Efficient Parallelized 3-D FNPF Numerical Wave Tank for Large-Scale Wave Basin Experiment Simulation", *J. Offshore Mech. and Arctic Engng*, 135:2.

Nouguier, F, Grilli, ST and Guérin, C-A (2014). "Nonlinear ocean wave reconstruction algorithms based on spatiotemporal data acquired by a flash LIDAR camera.", *IEEE Transactions on Geoscience and Remote Sensing*, 52(3), 1761-1771.

Raach, S, Schlipf, D, Sandner, F, Matha, D, and Cheng, PW (2014). "Nonlinear model predictive control of floating wind turbines with individual pitch control.", *Proc. 2014 American Control Conference*, IEEE, 4434-4439.

Verma, M, Nartu, MK, and Subbulakshmi, A (2022)."Optimal TMD design for floating offshore wind turbines considering model uncertainties and physical constraints.", *Ocean Engineering*, 243:110236.

Viselli, AM, Dagher, HJ, and Goupee, AJ (2015). "Model Test of a 1:8-scale Floating Wind Turbine Offshore in the Gulf of Maine.", *J. Offshore Mech. and Arctic Engng*, 137(4):041901-5.

Viselli, AM, Dagher, HJ, Goupee, AJ, and Allen, CK (2015). "Design and model confirmation of the intermediate scale Volturn US floating wind turbine subjected to its extreme design conditions.", *Wind Energy Journal*, 19(6):1161-1177.

Viselli AM, Forristall GZ, Pearce, B, and Dagher, HJ (2015). "Estimation of extreme wave and wind design parameters for offshore wind turbines in the Gulf of Maine using a POT method.", *Ocean Engineering*, 104:649-658.

Wakui, T, Nagamura, A, and Yokoyama, R (2021). "Stabilization of power output and platform motion of a floating offshore wind turbine-generator system using model predictive control based on previewed disturbances", *Renewable Energy*, 173, 105-127.